Supporting Information for

Identifying iron-nitrogen/carbon active structures for oxygen reduction reaction under the effect of electrode potential

Kun Mao, Lijun Yang*, Xizhang Wang, Qiang Wu and Zheng Hu

Key Laboratory of Mesoscopic Chemistry of MOE, School of Chemistry and Chemical Engineering, Nanjing University, Nanjing 210023, China

*Correspondence: lijunyang@nju.edu.cn

Table of Contents

Methods and Computational details

All the spin-unrestricted calculations in this study were performed with the package of DMol[3] at the density functional theory (DFT) level. The generalized gradient-corrected Perdew-Burke-Ernzerhof (PBE/GGA) functional, along with a double numerical basis set including *p*-polarization function (DNP), is applied for all calculations.[1] The core treatment is density functional semicore pseudopotential (DSPP), which includes some degree of relativistic correction. The solution effect of water was accounted by using conductor-like screening model (COSMO). Dispersion corrected DFT (DFT-D) scheme is used to describe the van der Waals (vdW) interaction. During the coordinates relaxation, the tolerances of energy and force were 1×10^{-5} Ha and 0.002 Ha/Å (1 Ha=27.2114eV), and the maximum displacement was 5×10^{-3} Å, respectively. The Monkhorst-Pack k-point mesh was set to be 4×4×1 and the global orbital cutoff was set as 5.0 Å.

The calculation of free energy diagram was performed according to the method proposed by Nørskov et al.[2] And the free energy was calculated by the equation G = E + ZPE − TS, where E is the total energy, ZPE is the zero-point energy, T is the room temperature in kelvin (298.15), and S is the entropy. The partial hessian method was used to determine the contributions of ZPE and entropy, which only calculate the vibrational frequencies of the adsorbate to save the computational cost.[3]

The free energy of $(H^+ + e^-)$ under standard conditions is taken to be $1/2H_2$. The free energy of O_2 was obtained from the reaction $O_2 + 2H_2 \rightarrow 2H_2O$, with a known free energy decrease of 4.92 eV. The free energy of H_2O (l) was derived from the equation G_{H2O} (l) = G_{H2O} (g) + RT × ln (p/p_0), where R is the ideal gas constant, T = 298.15 K, p = 0.035 bar, and p_0 = 1 bar.[4]

The activity of a structure is evaluated with its thermodynamic overpotential (η_{ORR}) and onset potential (U_{onset}), as calculated by Nørskov et al.[5] The onset potential is determined by the rate-limiting step of the elementary reactions of ORR, which is the step with minimum reaction free energy.[6]

$$U_{onset} = \min(\Delta G_1, \Delta G_2, \Delta G_3, \Delta G_4)/e \quad (1)$$

$$\eta_{ORR} = 1.23 - |U_{ORR}| \quad (2)$$

The (ΔG_1, ΔG_2, ΔG_3, ΔG_4) are the free energy changes of Reaction (10) - (13) (see S8.ORR processes on Fe-N/C), respectively.

S1. The constant potential method

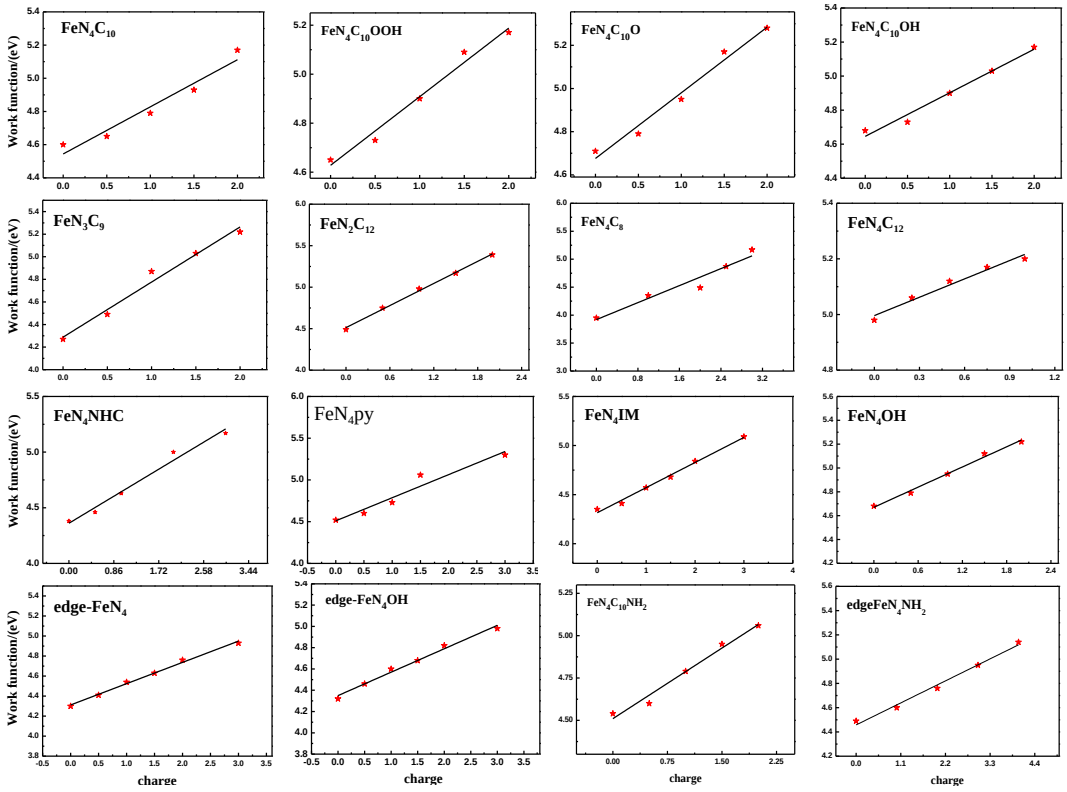

Figure S1 The relationships between work function and charge.

The relationship between electrode potential and work function of the electrode is[7]:

$$U/\mathrm{V} = (\Phi - 4.44)/\mathrm{eV} + 0.0592\ \mathrm{pH/V} \quad (3)$$

Where U is the electrode potential, Φ is the work function, 4.44 eV is the work function of the normal hydrogen electrode (NHE), and 0.0592 is the potential change by one pH unit. In this study, we set the pH = 1 to match the condition of PEMFCs. Thus the Φ at targeted U can be derived with equation (3). We then carried out work function calculations at five different charged states for each model in figure S1, and extrapolated the electron number e for the Φ at targeted U. The detailed data are shown in table S1.

Table S1. The net charges corresponding to electrode potentials for each structure

Structure	Relationship	Net charge				
		0 V	**0.2 V**	**0.4 V**	**0.6 V**	**0.8 V**
FeN_4C_8	$\Phi = 0.520\ Q + 3.873$	0.90	1.28	1.67	2.05	2.44
FeN_4C_{10}	$\Phi = 0.284\ Q + 4.544$	-0.49	0.01	0.69	1.40	2.10
FeN_4C_{12}	$\Phi = 0.220\ Q + 4.996$	-3.00	-2.07	-1.16	-0.25	0.65
FeN_2C_{12}	$\Phi = 0.444\ Q + 4.512$	-0.39	0.06	0.51	0.96	1.41
FeN_3C_9	$\Phi = 0.488\ Q + 4.288$	0.11	0.52	0.93	1.34	1.75
edge-FeN_4	$\Phi = 0.213\ Q + 4.312$	0.13	1.07	2.01	2.96	3.89
FeN_4PY	$\Phi = 0.277\ Q + 4.510$	-0.61	0.11	0.83	1.55	2.27
FeN_4IM	$\Phi = 0.256\ Q + 4.316$	0.09	0.88	1.65	2.44	3.22
FeN_4NHC	$\Phi = 0.282\ Q + 4.361$	-0.07	0.79	1.34	2.05	2.76
FeN_4OH	$\Phi = 0.282\ Q + 4.670$	-1.17	-0.46	0.25	0.96	1.67
edge-FeN_4OH	$\Phi = 0.220\ Q + 4.350$	-0.05	0.86	1.77	2.68	3.59
armchairNC	$\Phi = 0.266\ Q + 4.188$	0.57	1.32	2.07	2.83	3.58
zigzagNC	$\Phi = 0.282\ Q + 4.670$	-3.28	-1.0	1.17	3.39	5.61
graphiteNC	$\Phi = 0.282\ Q + 4.550$	-0.74	0.04	0.67	1.38	2.10
FeN_4NH_2	$\Phi = 0.278\ Q + 4.510$	-0.61	0.11	0.83	1.55	2.27
edge-FeN_4NH_2	$\Phi = 0.165\ Q + 4.458$	-0.72	0.5	1.71	2.92	4.13

S2. Constant charge corrections

In this study, we keep the potential constant among the pristine models by tuning the work function of each model, and charge constant during the ORR calculations. After the chemisorption of ORR intermediates, there will be some Φ variations, leading to the potential deviated from the targeted potential. We then use the method proposed by Goddard III and Norskov to correct the energy change caused by the deviated potential during ORR.[8-10] The best active site edge-FeN_4OH was chosen as the model system to perform the correction. The energy difference caused Φ variations is:

$$\Delta E_{\Phi_1-\Phi_2} = E_{\Phi_1} - E_{\Phi_2} = \frac{\Delta q \times \Delta \Phi}{2} \quad (4)$$

The Δq and ΔΦ are the interfacial charge and work function difference between the states of pristine and adsorbed. Since the interfacial charge difference is hard to be accurately obtained, we can use the capacitance (C) defined in formula (5) to replace Δq:

$$C = \frac{\Delta q}{\Delta \Phi} \quad (5)$$

$$\Delta q = C \times \Delta \Phi \quad (6)$$

Where the 1/C is the slope of the work function-charge relationship. We then substitute the Δq in (4) with (6):

$$\Delta E_{\Phi_1-\Phi_2} = \frac{C \times \Delta \Phi^2}{2} \quad (7)$$

Here, the C of each ORR intermediate steps for edge-FeN_4OH were listed in column of 'relationship' in table S2 and the free energy corrections (ΔE) were listed in table S3. We found that the energy variations at high electrode potential range (0.4 - 0.8V) are tinny enough (< 0.04 eV) to be ignored and it has little effect (~0.1 eV) on the activity in the low electrode potential range (0V - 0.4V). We don't think the energy variation will affect the activity order and there is no need to extrapolate the *e* for each chemisorbed states in this study.

Table S2. The work function-charge relationship and net charge of edge-FeN_4OH intermediate structures at different electrode potential.(*: edge-FeN_4OH)

Structure	Relationship	Net charge				
		0 V	**0.2 V**	**0.4 V**	**0.6 V**	**0.8 V**
*	$\Phi = 0.220\ Q + 4.35$	0.0	0.9	1.8	2.7	3.6
*OOH	$\Phi = 0.160\ Q + 4.60$	-1.4	-0.1	1.1	2.4	3.6
*O	$\Phi = 0.166\ Q + 4.57$	-1.1	0.0	1.3	2.5	3.7
*OH	$\Phi = 0.150\ Q + 4.60$	-1.5	-0.1	1.2	2.5	3.9

Table S3. The work function (Φ) and free energy corrections (ΔE) for the ORR intermediate step at different eletrode potentials.

U (V)	Φ_* (eV)	Φ_{*OOH}(eV)	Φ_{*O}(eV)	Φ_{*OH}(eV)	ΔE_{*OOH-*}(eV)	ΔE_{*O-*}(eV)	ΔE_{*OH-*}(eV)
0	4.35	4.60	4.57	4.60	0.141	0.109	0.141
0.2	4.55	4.74	4.72	4.73	0.081	0.065	0.073
0.4	4.75	4.88	4.87	4.87	0.038	0.032	0.032
0.6	4.95	5.03	5.02	5.01	0.014	0.011	0.008
0.8	5.15	5.17	5.18	5.14	0.001	0.002	0.000

S3. The models of edge-hosted structures

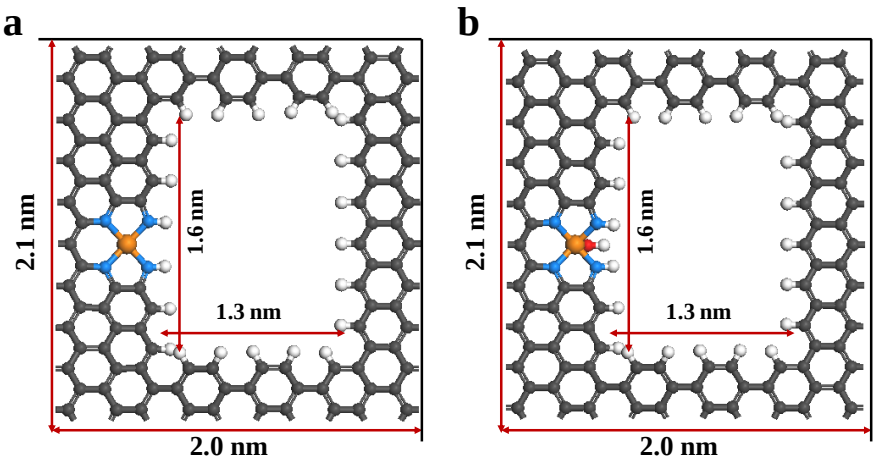

Figure S2. The models of edge-FeN_4 (a) and edge-FeN_4OH (b), which were partially displayed in Figure 1 in the main text.

S4. Calculation of exchange current density

The exchange current density for a certain electrocatalytic processes can be calculated with equation (8)[11, 12].

$$j = e\rho TOF_{e^-} \tag{8}$$

Where j is the current density at the corresponding electrode potential, where e is the elementary charge and ρ is the surface density of active sites and TOF_{e^-} is the turn over frequency. Here ρ is 3.2×10^{16} sites/cm^2 according to the recent report for the accurate evaluation of active-site density of Fe-N/C ORR electrocastalysts[13]. TOF_{e^-} can be inferred through equation (9) at steady state[14, 15].

$$k_i = A_i \exp\left(-\frac{E_{a,i}}{k_B T}\right)\exp\left(-\frac{e\beta_i\left(U - U_i\right)}{k_B T}\right) \tag{9}$$

Where U_i is the reversible potential of step i deduced by the maximum of the four ORR free-energy steps, and U is the intrinsic onset potential of each moiety. K_B is Boltzmann constant, and T is temperature (298.15 K). A_i is the effective pre-exponential factor estimated as 10^9 s^{-1}, and β is the symmetric factor taken as 0.5. $E_{a,i}$ of 0.25 eV was used since the kinetic barriers of adsorption-desorption step on the slab surface are generally around this value[16].

S5. Calculation of intrinsic onset potentials

The intrinsic onset potentials (U_{onset}) of each active structure are derived from the potential value at G=0 eV. The equilibrium potentials in figure S3 are derived from Figure S4 (a-e) and listed in table S4, which is minimum of the four ORR free-energy steps (ΔG_{min}).

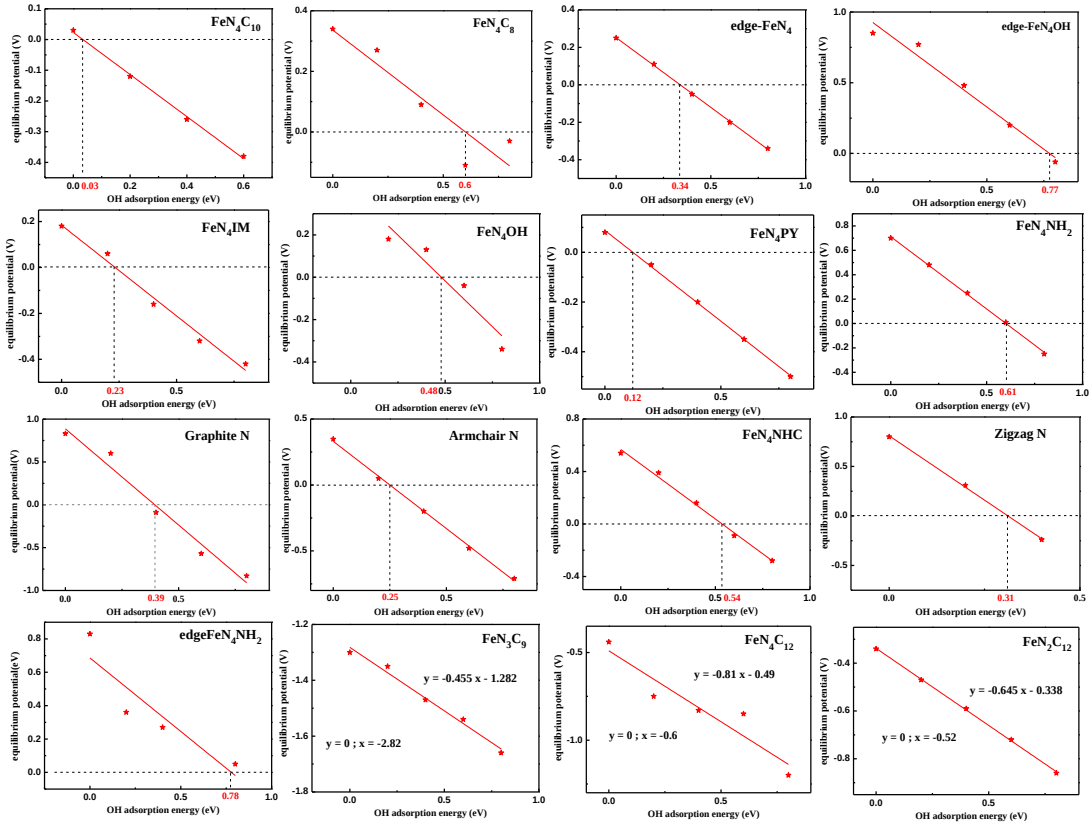

Figure S3 Locating the intrinsic onset potential of each structure.

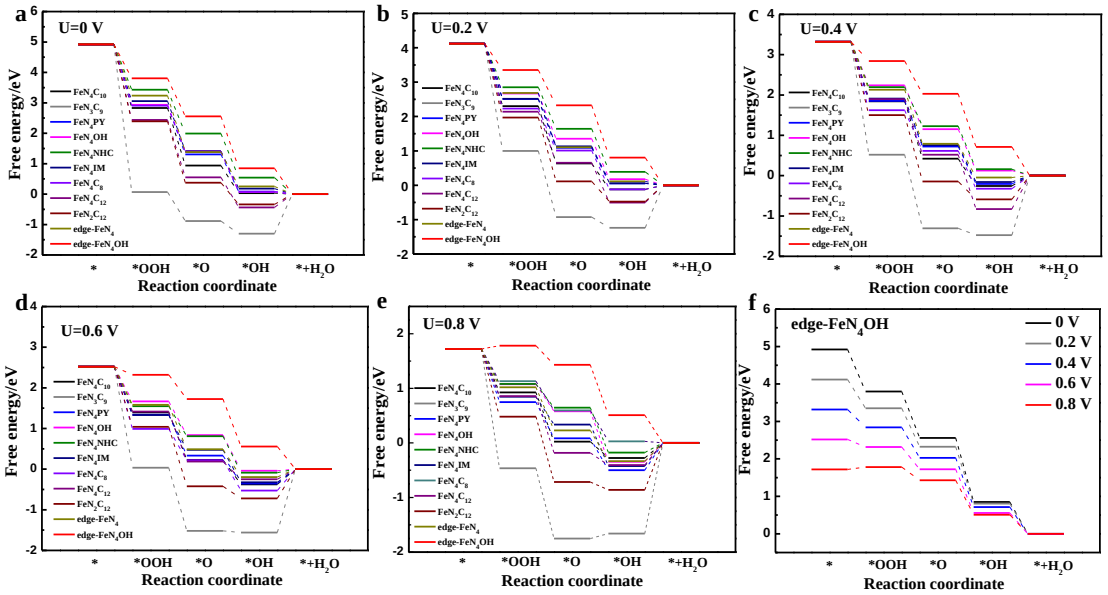

Figure S4 Free energy curves of eleven structures at different electrode potentials (a) U = 0 V, (b) U = 0.2 V, (c) U = 0.4 V, (d) U = 0.6 V, (e) U = 0.8 V, (f) the free energy of edge-FeN_4OH at each electrode potential.

Table S4 ΔG_{min} of each structure at 0V-0.8 V (vs RHE)

Structure	ΔGmin (eV)				
	0 V	0.2 V	0.4 V	0.6 V	0.8 V
edge-FeN_4OH	-0.85	-0.77	-0.48	-0.2	0.06
FeN_4C_8	-0.34	-0.27	-0.09	0.11	0.03
FeN_4NHC	-0.54	-0.39	-0.16	0.09	0.28
FeN_4OH	-0.37	-0.28	-0.13	0.04	0.34
edge-FeN_4	-0.25	-0.11	0.05	0.2	0.34
FeN_4PY	-0.08	-0.05	0.2	0.35	0.5
FeN_4IM	-0.18	-0.06	0.16	0.32	0.42
FeN_4C_{10}	-0.03	0.12	0.26	0.38	0.28
FeN_2C_{12}	0.34	0.47	0.59	0.72	0.86
FeN_4C_{12}	0.44	0.50	0.83	0.25	0.4
FeN_3C_9	1.3	1.24	1.47	1.54	1.66
armchair NC	-0.35	-0.05	0.20	0.48	0.71
zigzag NC	-0.80	-0.31	0.24	0.20	0.14
graphite NC	-0.83	-0.60	0.09	0.57	0.83

FeN_4NH_2	-0.49	-0.48	-0.25	-0.01	0.25

Table S5 Intrinsic Onset Potential(Intrinsic U_{onset}) of the eleven structures

Structure	Intrinsic U_{onset} (V)
edge-FeN_4OH	0.75
FeN_4C_8	0.60
FeN_4NHC	0.54
FeN_4OH	0.48
edge-FeN_4	0.34
FeN_4PY	0.12
FeN_4C_{10}	0.03
FeN_2C_{12}	-0.52
FeN_4IM	0.23
FeN_4C_{12}	-0.60
FeN_3C_9	-2.82

S6. The calculation of Ed

We use the following formula (10) to calculate the center of the d band[17, 18]

$$Ed = \frac{\int_{-\infty}^{0} ED(E)dE}{\int_{-\infty}^{0} D(E)dE} \quad (10)$$

Where E_d is the energy at the center of the d band, D(E) is the DOS of d-band at a given energy E. The d band density of states (DOS) curve of the six structures are plotted in Figure S5 and the calculated E_d are listed in table S6.

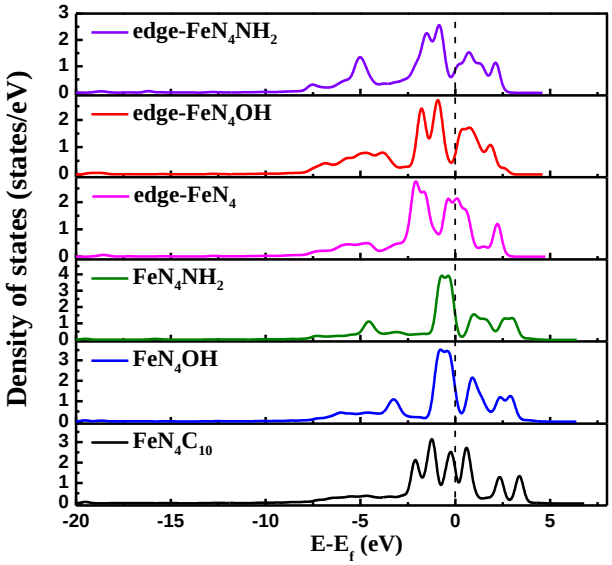

Figure S5. The d-band density of states (DOS) for the six structures in figure 4a.

Table S6 The calculated E_d of six structures in firgure 4a

Structure	E_d (eV)
FeN_4C_{10}	-1.68
FeN_4OH	-1.75
FeN_4NH_2	-1.96
edge-FeN_4	-1.97
edge-FeN_4OH	-2.18
edge-FeN_4 NH_2	-2.94

S7. Comparison for O_2 adsorption energies

Table S7 O_2 adsorption energy of metal-free and Fe-N/C structures

Structures	E_{abs} (eV)
Armchair	0.45
Zigzag	-0.44
Graphite	-0.7
FeN_4NHC	-0.77
edge-FeN_4	-0.84
edge-FeN_4OH	-0.97
FeN_4IM	-0.98
FeN_4NH_2	-1.17
FeN_4OH	-1.18
FeN_4PY	-1.18
FeN_2C_{12}	-1.34
FeN_4C_8	-1.35
FeN_4C_{10}	-1.39
FeN_4C_{12}	-1.69

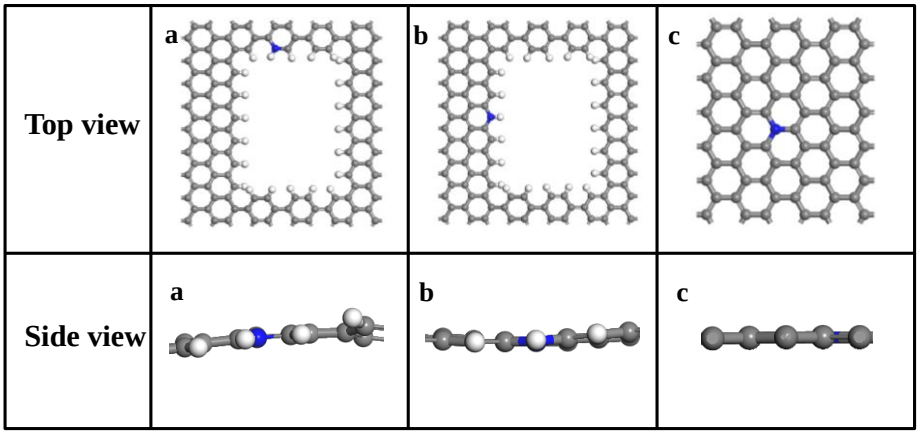

Figure S6 Metal-free structures (a) armchair N/C; (b) zig-zag N/C; (c) graphite N/C.

S8. ORR processes on Fe-N/C

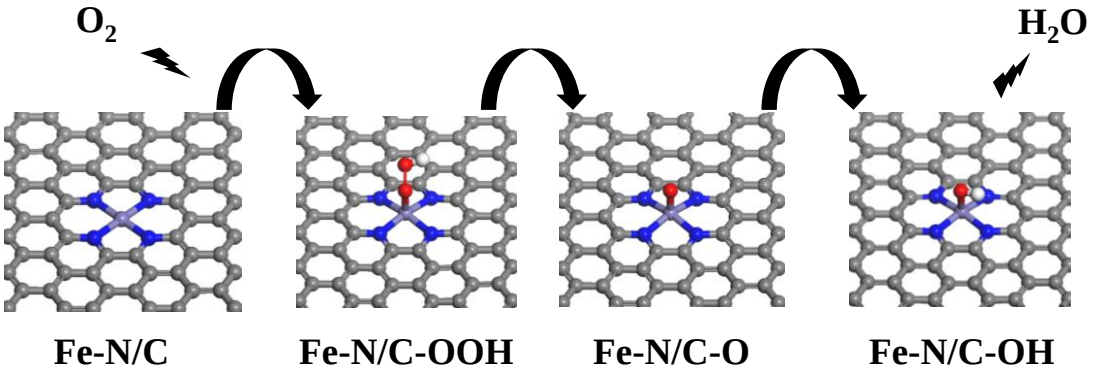

Figure S7 The four electron ORR pathway on Fe-N/C.

The complete $4e^-$ ORR process in acid medium is described by equations (10)-(13). The asterisk (*) indicates the adsorption sites or the species in chemisorbed state. The calculated free energy changes (ΔG) for each ORR step are denoted as ΔG_1-ΔG_4, respectively.

$$O_2 + 4H^+ + e^- + * \rightarrow OOH* + 3H^+ \quad (10)$$

$$OOH* + 3H^+ + e^- \rightarrow O* + 2H^+ + H_2O \quad (11)$$

$$O* + 2H^+ + H_2O + e^- \rightarrow OH* + H_2O + e^- \quad (12)$$

$$OH* + H_2O + H^+ + e^- \rightarrow 2H_2O + * \quad (13)$$

S9. The free energy data for all structures

In table S8, we listed the free energy values corresponding to the elemental reactions in each step of the ORR process of all configurations at the potentials of 0V - 0.8 V.

Table S8. The free energy values of the ORR process of all structures involved in this study at the potential from 0V to 0.8V

graphite N/C					
Potential(V)	*(eV)	*OOH(eV)	*O(eV)	*OH(eV)	*(eV)
0	4.92	3.88	1.66	0.83	0.00
0.2	4.12	3.52	2.11	0.85	0.00
0.4	3.32	3.41	2.34	1.12	0.00
0.6	2.52	3.09	2.06	1.22	0.00
0.8	1.72	2.55	1.75	1.09	0.00
armchair N/C					
Potential(V)	*(eV)	*OOH(eV)	*O(eV)	*OH(eV)	*(eV)
0	4.92	4.57	2.69	1.30	0.00
0.2	4.12	4.07	2.50	1.19	0.00
0.4	3.32	3.52	2.34	1.12	0.00
0.6	2.52	3.00	2.16	1.05	0.00
0.8	1.72	2.43	1.94	0.96	0.00
zig-zag N/C					
Potential(V)	*(eV)	*OOH(eV)	*O(eV)	*OH(eV)	*(eV)
0	4.92	3.71	2.36	0.80	0.00
0.2	4.12	3.76	1.73	1.42	0.00
0.4	3.32	2.86	1.44	1.68	0.00
0.6	2.52	2.11	1.30	1.50	0.00
0.8	1.72	1.61	1.20	1.34	0.00
FeN_4NH_2					
Potential(V)	*(eV)	*OOH(eV)	*O(eV)	*OH(eV)	*(eV)
0	4.92	3.37	1.96	0.49	0.00
0.2	4.12	2.99	1.78	0.48	0.00
0.4	3.32	2.38	1.40	0.25	0.00
0.6	2.52	1.65	0.98	0.01	0.00
0.8	1.72	1.08	0.64	-0.25	0.00

FeN_4NO_2

Potential(V)	*(eV)	*OOH(eV)	*O(eV)	*OH(eV)	*(eV)
0	4.92	3.16	1.66	0.30	0.00
0.2	4.12	2.68	1.40	0.21	0.00
0.4	3.32	2.16	1.10	0.08	0.00
0.6	2.52	1.54	0.72	-0.13	0.00
0.8	1.72	1.01	0.46	-0.25	0.00

FeN_4C_8

Potential(V)	*(eV)	*OOH(eV)	*O(eV)	*OH(eV)	*(eV)
0	4.92	3.22	1.39	0.34	0.00
0.2	4.12	2.71	1.08	0.27	0.00
0.4	3.32	2.34	0.86	0.09	0.00
0.6	2.52	1.74	0.46	-0.11	0.00
0.8	1.72	0.98	0.10	-0.03	0.00

FeN_4C_{12}

Potential(V)	*(eV)	*OOH(eV)	*O(eV)	*OH(eV)	*(eV)
0	4.92	2.38	0.82	-0.23	0.00
0.2	4.12	1.98	0.61	-0.34	0.00
0.4	3.32	1.68	0.50	-0.32	0.00
0.6	2.52	1.35	0.36	-0.38	0.00
0.8	1.72	0.86	0.13	-0.58	0.00

FeN_4C_{10}

Potential(V)	*(eV)	*OOH(eV)	*O(eV)	*OH(eV)	*(eV)
0	4.92	2.83	0.94	0.03	0.00
0.2	4.12	2.30	0.63	-0.12	0.00
0.4	3.32	1.84	0.42	-0.26	0.00
0.6	2.52	1.40	0.23	-0.38	0.00
0.8	1.72	0.92	0.02	-0.28	0.00

FeN_2C_{12}

Potential(V)	*(eV)	*OOH(eV)	*O(eV)	*OH(eV)	*(eV)
0	4.92	2.44	0.37	-0.34	0.00
0.2	4.12	1.97	0.11	-0.47	0.00
0.4	3.32	1.50	-0.15	-0.59	0.00
0.6	2.52	1.04	-0.42	-0.72	0.00
0.8	1.72	0.48	-0.72	-0.86	0.00

FeN_3C_9					
Potential(V)	*(eV)	*OOH(eV)	*O(eV)	*OH(eV)	*(eV)
0	4.92	0.07	-0.88	-1.3	0.00
0.2	4.12	1.00	-0.92	-1.24	0.00
0.4	3.32	0.52	-1.31	-1.47	0.00
0.6	2.52	0.03	-1.52	-1.56	0.00
0.8	1.72	-0.46	-1.75	-1.66	0.00
edge-FeN_4					
Potential(V)	*(eV)	*OOH(eV)	*O(eV)	*OH(eV)	*(eV)
0	4.92	3.24	1.38	0.25	0.00
0.2	4.12	2.69	1.10	0.11	0.00
0.4	3.32	2.13	0.79	-0.05	0.00
0.6	2.52	1.58	0.49	-0.20	0.00
0.8	1.72	1.02	0.23	-0.34	0.00
FeN_4PY					
Potential(V)	*(eV)	*OOH(eV)	*O(eV)	*OH(eV)	*(eV)
0	4.92	2.93	1.3	0.08	0.00
0.2	4.12	2.51	1.09	0.05	0.00
0.4	3.32	1.85	0.72	-0.20	0.00
0.6	2.52	1.34	0.33	-0.35	0.00
0.8	1.72	0.75	0.09	-0.50	0.00
FeN_4OH					
Potential(V)	*(eV)	*OOH(eV)	*O(eV)	*OH(eV)	*(eV)
0	4.92	2.94	1.41	0.57	0.00
0.2	4.12	2.67	1.35	0.28	0.00
0.4	3.32	2.24	1.15	0.13	0.00
0.6	2.52	1.67	0.84	-0.04	0.00
0.8	1.72	1.08	0.58	-0.34	0.00
FeN_4NHC					
Potential(V)	*(eV)	*OOH(eV)	*O(eV)	*OH(eV)	*(eV)
0	4.92	3.43	1.99	0.54	0.00
0.2	4.12	2.85	1.64	0.39	0.00
0.4	3.32	2.20	1.23	0.16	0.00
0.6	2.52	1.55	0.81	-0.09	0.00
0.8	1.72	1.08	0.65	-0.18	0.00

FeN_4IM					
Potential(V)	*(eV)	*OOH(eV)	*O(eV)	*OH(eV)	*(eV)
0	4.92	3.06	1.41	0.18	0.00
0.2	4.12	2.52	1.13	0.06	0.00
0.4	3.32	1.91	0.76	-0.16	0.00
0.6	2.52	1.33	0.47	-0.32	0.00
0.8	1.72	0.85	0.34	-0.42	0.00
edge-FeN_4OH					
Potential(V)	*(eV)	*OOH(eV)	*O(eV)	*OH(eV)	*(eV)
0	4.92	3.8	2.56	0.85	0.00
0.2	4.12	3.35	2.33	0.81	0.00
0.4	3.32	2.84	2.03	0.71	0.00
0.6	2.52	2.32	1.72	0.56	0.00
0.8	1.72	1.78	1.43	0.51	0.00

Reference

(1) Perdew, J. P.; Burke, K.; Ernzerhof, M. Generalized Gradient Approximation Made Simple. *Phys. Rev. Lett*. **1996**, *77*, 3865.

(2) Hansen, H. A.; Rossmeisl, J.; Norskov, J. K. Surface Pourbaix diagrams and oxygen reduction activity of Pt, Ag and Ni(111) surfaces studied by DFT. Phys. *Chem. Chem. Phys*. **2008**, *10*, 3722-3730.

(3) Acharya, C. K.; Turner, C. H. CO oxidation with Pt (111) supported on pure and boron-doped carbon: A DFT investigation. *Surface. Sci*. **2008**, *602*, 3595-3602

(4) Jiang, Y.; Yang, L.; Sun, T.; Zhao, J.; Lyu, Z.; Zhuo, O.; Wang, X.; Wu, Q.; Ma, J.; Hu, Z. Significant Contribution of Intrinsic Carbon Defects to Oxygen Reduction Activity. *ACS. Catal.* **2015**, *5* (11), 6707-6712.

(5) Nørskov, J. K.; Rossmeisl, J.; Logadottir, A.; Lindqvist, L.; Kitchin, J. R.; Bligaard, T. Origin of the Overpotential for Oxygen Reduction at a Fuel-Cell Cathode. *J. Phys. Chem. B*. **2004**, *108*(46), 17886-17892

(6) Zhao, Z.; Li, M.; Zhang, L.; Dai, L. Xia, Z. Design Principles for Heteroatom-Doped Carbon Nanomaterials as Highly Effi cient Catalysts for Fuel Cells and Metal-Air Batteries. *Adv. Mater*. **2015**, *27*, 6834-6840

(7) Wang, X.; Chen, Z.; Zhao, X.; Yao, T.; Chen, W.; You, R.; Zhao, C.; Wu, G.; Wang, J.; Huang, W.; Yang, J.; Hong, X.; Wei, S.; Wu, Y.; Li, Y. Regulation of Coordination Number over Single Co Sites Triggers the Efficient Electroreduction of CO_2. *Angew. Chem. Int. Ed*. **2018**, *57* (7), 1944-1948.

(8) Cheng, T.; Xiao, H.; Goddard III, W. A. Reaction Mechanisms for the Electrochemical Reduction of CO_2 to CO and Formate on the Cu(100) Surface at 298K from Quantum Mechanics Free Energy Calculations with Explicit Water. *J. Am. Chem. Soc.* **2016**, *138*(42):13802-13805.

(9) Chan, K.; Norskov, J. K. Electrochemical Barriers Made Simple. *J, Phys, Chem, Lett.* **2015**, *6* (14), 2663-8.

(10) Chan, K.; Norskov, J. K. Potential Dependence of Electrochemical Barriers from ab Initio Calculations. *J, Phys, Chem, Lett.* **2016**, *7* (9), 1686-90.

(11) Nørskov, J. K.; Rossmeisl, J.; Logadottir, A.; Lindqvist, L.; Kitchin, J. R.; Bligaard, T. Origin of the Overpotential for Oxygen Reduction at a Fuel-Cell Cathode. *J. Phys. Chem. B*. **2004**, *108*(46), 17886-17892.

(12) Wang, Y.; Li, Y.; Heine, T. PtTe Monolayer: Two-Dimensional Electrocatalyst with High Basal Plane Activity toward Oxygen Reduction Reaction. *J. Am. Chem. Soc*. **2018**, *140*, 12732.

(13) Luo, F.; Choi, C. H.; Primbs, M. J. M. Accurate Evaluation of Active-Site Density (SD) and Turnover Frequency (TOF) of PGM-Free Metal−Nitrogen-Doped Carbon (MNC) Electrocatalysts using CO Cryo Adsorption. *ACS. Catal.* **2019**, *9*, 4841-4852.

(14) Wang, Y.; Tang, Y.; Zhou, K. Self-Adjusting Activity Induced by Intrinsic Reaction Intermediate in Fe-N-C Single-Atom Catalysts. *J. Am. Chem. Soc*. **2019**, *141*, 14115-14119.

(15) Hansen, H. A.; Viswanathan, V.; Nørskov, J. K. Unifying Kinetic and Thermodynamic Analysis of 2 e^- and 4 e^- Reduction of Oxygen on Metal Surfaces. *J. Phys. Chem. C*. **2014**, *118*, 6706-

6718.

(16) Jiao, Y.; Zheng, Y.; Jaroniec, M.; Qiao, S. Z. Origin of the Electrocatalytic Oxygen Reduction Activity of Graphene-Based Catalysts: A Roadmap to Achieve the Best Performance. *J. Am. Chem. Soc.* **2014**, *136* (11), 4394-403.

(17) Song, Q.; Li, J.; Wang, S.; Liu, J.; Liu, X.; Pang, L.; Li, H.; Liu, H. Enhanced Electrocatalytic Performance through Body Enrichment of Co-Based Bimetallic Nanoparticles In Situ Embedded Porous N-Doped Carbon Spheres. *Small.* **2019**, *15*, 1903395.

(18) Pei, W.; Zhou, S.; Bai, Y.; Zhao, J. N-doped graphitic carbon materials hybridized with transition metals (compounds) for hydrogen evolution reaction: Understanding the synergistic effect from atomistic level. *Carbon*. **2018**, *133*, 260-266